Heat conduction in one-dimensional lattices with on-site potential

A. V. Savin* and O. V. Gendelman†
Institute of Chemical Physics, RAS, Kosygin Street 4, Moscow, Russia
(Received 30 April 2002; revised manuscript received 11 February 2003; published 24 April 2003)

The process of heat conduction in one-dimensional lattices with on-site potential is studied by means of numerical simulation. Using the discrete Frenkel-Kontorova, ϕ^4, and sinh-Gordon models we demonstrate that contrary to previously expressed opinions the sole anharmonicity of the on-site potential is insufficient to ensure the normal heat conductivity in these systems. The character of the heat conduction is determined by the spectrum of nonlinear excitations peculiar for every given model and therefore depends on the concrete potential shape and the temperature of the lattice. The reason is that the peculiarities of the nonlinear excitations and their interactions prescribe the energy scattering mechanism in each model. For sine-Gordon and ϕ^4 models, phonons are scattered at a dynamical lattice of topological solitons; for sinh-Gordon and for ϕ^4 in a different parameter regime the phonons are scattered at localized high-frequency breathers (in the case of ϕ^4 the scattering mechanism switches with the growth of the temperature).

DOI: 10.1103/PhysRevE.67.041205 PACS number(s): 44.10.+i, 05.45.−a, 05.60.−k, 05.70.Ln

I. INTRODUCTION

Heat conductivity in one-dimensional (1D) lattices is a well known classical problem related to the microscopic foundation of Fourier's law. The problem started from the famous work of Fermi, Pasta, and Ulam (FPU) [1], where an abnormal process of heat transfer was detected for the first time. Nonintegrability of the system is a necessary condition for normal heat conductivity. As it was demonstrated recently for the FPU lattice [2–4], disordered harmonic chain [5–7], diatomic 1D gas of colliding particles [8–11], and the diatomic Toda lattice [12], the nonintegrability is not sufficient in order to get normal heat conductivity. It leads to a linear distribution of temperature along the chain for small gradient, but the value of heat flux is proportional to $1/N^{\alpha}$, where $0<\alpha<1$ and N is the number of particles in the chain. Thus, the coefficient of heat conductivity diverges in the thermodynamic limit $N\rightarrow\infty$. Analytical estimations [4] have demonstrated that any chain possessing an acoustic phonon branch should have infinite heat conductivity in the limit of low temperatures.

From the other side, there are some artificial systems with on-site potential having normal heat conductivity [13,14]. The heat conductivity of the Frenkel-Kontorova chain was first considered in Ref. [15]. Finite heat conductivity for certain parameters was obtained for Frenkel-Kontorova chain [16], for the chain with sinh-Gordon on-site potential [17], and for the chain with ϕ^4 on-site potential [18,19]. These models are not invariant with respect to translation and the momentum is not conserved. It was supposed that the on-site potential is extremely significant for normal heat conduction [18] and that the anharmonicity of the on-site potential is sufficient to ensure the validity of Fourier's law [20]. A recent detailed review of the problem is presented in Ref. [21].

The behavior of the heat conduction of the Frenkel-Kontorova model for all parameters and temperatures is not known. Chains with zero average pressure were demonstrated to have normal heat conductivity [22–24]. In papers [23,24] the transition from abnormal to normal heat conductivity has been detected at a certain temperature.

There are no detailed investigations similar to the ones mentioned above and concerning the properties of the chains with on-site potential in the whole temperature range. As it was mentioned above, our knowledge is incomplete concerning even the most popular and paradigmatic discrete Frenkel-Kontorova chain. This lattice is of special interest as its counterpart in the continuous limit is the famous sine-Gordon system (having, of course, divergent heat conductivity).

A question of special interest is also the mechanism of phonon (or soliton) scattering which gives rise to finite heat conductivity. For the chain with periodic nearest-neighbor interaction it was demonstrated [23,24] that the transition to normal heat conductivity corresponds to abrupt growth of concentration of rotation solitons (rotobreathers), demonstrating certain similarity with phase transition. Namely, the transition temperature corresponds to region of maximum heat capacity of the lattice. Similarly, it is reasonable to investigate whether such relationship between the heat capacity and the heat conductivity is peculiar also for other models of the nonlinear chains.

The paper is devoted to the detailed simulation of discrete lattices with on-site nonlinearity and quadratic potential of nearest-neighbor interaction and investigation of their heat conductivity. The lattices are Frenkel-Kontorova, sinh-Gordon, and discrete ϕ^4. For every case the dependence of the heat conductivity on the temperature and on the parameters of the lattice will be explored, and concrete elementary excitations responsible for the change of regimes will be revealed.

II. DESCRIPTION OF THE MODEL

Let us consider a one-dimensional atomic chain arranged along the x axis. All particles are of equal mass M, and the nearest-neighbor interaction is described by a harmonic po-

*Email address: asavin@center.chph.ras.ru
†Email address: ovgend@center.chph.ras.ru

tential with rigidity K. Then the Hamiltonian of the lattice will take a form

$$\mathcal{H}=\sum_n \left\{\frac{1}{2}M\dot{x}_n^2+\frac{1}{2}K(x_{n+1}-x_n)^2+U(x_n)\right\}, \qquad (1)$$

where the dot denotes the differentiation with respect to time t, x_n is the displacement of the nth particle from its equilibrium position, and $U(x)$ is an on-site potential.

The dimensionless variables are introduced as $u_n=2\pi x_n/a$ (a is the equilibrium distance between the particles) for the displacement, $\tau=t\sqrt{K/M}$ for the time and $H=4\pi^2\mathcal{H}/Ka^2$ for the energy. Hamiltonian (1) takes the form

$$H=\sum_n \left\{\frac{1}{2}u_n'^2+\frac{1}{2}(u_{n+1}-u_n)^2+V(u_n)\right\}, \qquad (2)$$

where the prime denotes the differentiation with respect to the dimensionless time τ and the dimensionless on-site potential is introduced as $V(u_n)=4\pi^2U(au_n/2\pi)/Ka^2$. Natural definition for the dimensionless temperature is $T=4\pi^2k_B\Theta/Ka^2$, where k_B is Boltzmann constant, and Θ is the temperature in common units.

We are going to consider four widely used models for on-site potential: harmonic potential

$$V(u)=\frac{1}{2}\omega_0^2u^2, \qquad (3)$$

sine-Gordon potential

$$V(u)=\epsilon[1+\cos(u)], \qquad (4)$$

ϕ^4 potential

$$V(u)=2\epsilon[(u/\pi)^2-1]^2, \qquad (5)$$

and sinh-Gordon potential

$$V(u)=\omega_0^2[\cosh(u)-1]. \qquad (6)$$

Parameter $\epsilon>0$ determines the value of potential barrier between neighboring wells and its inverse $g=1/\epsilon$ characterizes the cooperativity of dynamics of chain's particles. Potentials (4) and (5) have the same distance between neighboring wells equal to 2π and equal value of the potential barrier 2ϵ. The parameter ω_0 in (3) and (6) corresponds to the minimal frequency of harmonic vibrations of the lattice.

III. METHODS FOR COMPUTATION OF THE HEAT CONDUCTION COEFFICIENT

The goal is to simulate the process of heat conduction in a finite chain containing N particles. For this purpose the left side of the chain ($n\leqslant 0$) has to be connected to a thermostat with temperature T_+, and the right side ($n>N$) to a thermostat with temperature T_- ($T_+>T_-$). For the purpose of the simulation we consider the chain of N_++N+N_- particles, where the first N_+ particles are attached to the thermostat T_+, an the last N_- particles to the thermostat T_- (Fig. 1). The potential of the nearest-neighbor interaction is

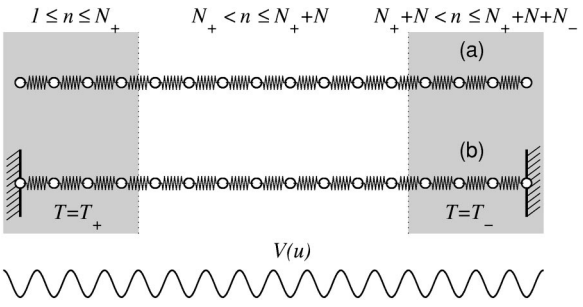

FIG. 1. Model of the chain of N_++N+N_- particles with left N_+ particles attached to the $T=T_+$ thermostat and right N_- particles attached to the $T=T_-$ thermostat. Boundary conditions correspond to free (a) and fixed (b) end particles. The potential $V(u)$ corresponds to the discrete Frenkel-Kontorova model.

harmonic, therefore the equilibrium length of the chain does not depend on the temperature. It implies that the boundary conditions at the ends of the lattice have no noticeable effect on the process of heat conduction and both the conditions of free [Fig. 1(a)] and fixed end particles [Fig. 1(b)] may be used. Numerical simulations with $N_\pm=40$ have demonstrated that there is no dependence on the choice of boundary conditions. We will use the condition of free ends with $N_\pm=40$ for all simulations.

The majority of papers devoted to heat conduction [2,3,16,18] use deterministic Nosé-Hoover thermostat [25] with $N_+=N_-=1$. However, this thermostat has been designed for the description of the thermalized system in the state of equilibrium and is not universally suitable for the description of nonequilibrium processes. Therefore we choose the well-known stochastic Langevin thermostat. Detailed comparison of these two thermostats is presented in section 3 of the Appendix.

Let us consider the chain with free ends ($1<n<N+N_++N_-$) with $N_\pm$ particles at both ends attached to Langevin thermostats. The dynamics of the system is described by equations

$$\begin{gathered}
u_n''=u_{n+1}-u_n-F(u_n)-\gamma u_n'+\xi_n^+,\\
n=1,\\
u_n''=u_{n+1}-2u_n+u_{n-1}-F(u_n)-\gamma u_n'+\xi_n^+,\\
n=2,\ldots,N_+,\\
u_n''=u_{n+1}-2u_n+u_{n-1}-F(u_n), \qquad (7)\\
n=N_++1,\ldots,N_++N,\\
u_n''=u_{n+1}-2u_n+u_{n-1}-F(u_n)-\gamma u_n'+\xi_n^-,\\
n=N_++N+1,\ldots,N_++N+N_--1,\\
u_n''=u_{n-1}-u_n-F(u_n)-\gamma u_n'+\xi_n^-,\\
n=N_++N+N_-,
\end{gathered}$$

where $F(u)=dU(u)/du$, the damping coefficient $\gamma=1/\tau_r$, τ_r is the characteristic relaxation time of the particles attached to the thermostat, $\xi_n^{\pm}$ is the random external force corresponding to Gaussian white noise normalized as

$$\langle \xi_n^{\pm}(\tau)\rangle = \langle \xi_n^{\pm}(\tau_1)\xi_k^{\mp}(\tau_2)\rangle = 0,$$

$$\langle \xi_n^{\pm}(\tau_1)\xi_k^{\pm}(\tau_2)\rangle = 2\gamma T_{\pm}\delta_{nk}\delta(\tau_2-\tau_1).$$

Details of numerical realization of the Langevin thermostat and random forces are presented in the Appendix.

At every moment the dimensionless temperature of the nth particle $t_n(\tau)=u_n'^2(\tau)$. In order to determine the value of the local heat flux j_n the energy distribution among the particles of the chain is considered:

$$h_n=\frac{1}{2}\left[\frac{1}{2}(u_n'^2+u_{n+1}'^2)+V(u_n)+V(u_{n+1})+(u_{n+1}-u_n)^2\right]. \tag{8}$$

By differentiating Eq. (8) with respect to time τ we get

$$h_n'=\frac{1}{2}\{u_n'[u_n''+F(u_n)]+u_{n+1}'[u_{n+1}''+F(u_{n+1})]\}$$

$$+(u_{n+1}-u_n)(u_{n+1}'-u_n').$$

Taking into account Eq. (7), we obtain

$$h_n'=\frac{1}{2}[u_{n+1}'(u_{n+2}-u_n)-u_n'(u_{n+1}-u_{n-1})]. \tag{9}$$

Taking into account the continuity condition $h_n'=j_n-j_{n-1}$ we get the expression for the energy flux: $j_n=-u_n'(u_{n+1}-u_{n-1})/2$.

System of equations (7) has been integrated numerically. We used the values of $\gamma=0.1$, $N_{\pm}=40$, $N=10$, 20, 40, 80, 160, 320, 640, and initial conditions corresponding to the ground state of the chain. After the time $\tau=10^5$ has elapsed, the end particles achieved thermal equilibrium with the thermostat and stationary heat flux has been formed. Afterwards, the dynamics of system (7) has been simulated at the time scale of order $\tau=10^7$. The average temperature of the particles,

$$T_n=\langle t_n(\tau)\rangle_{\tau}=\lim_{\tau\to\infty}\frac{1}{\tau}\int_0^{\tau}u_n'^2(s)ds, \tag{10}$$

and average value of the heat flux,

$$J_n=\langle j_n(\tau)\rangle_{\tau}=\lim_{\tau\to\infty}\frac{1}{\tau}\int_0^{\tau}j_n(s)ds, \tag{11}$$

were computed for the fragment of the chain between the thermostats.

If the temperature gradient $\Delta T=T_+-T_-$ is small, this method avoids the temperature jumps at the ends of the free fragment of the chain [27]. Characteristic distributions of the heat flux J_n and local temperature T_n are demonstrated at Fig. 2. At the inner fragment of the chain $N_+<n\leqslant N_++N$

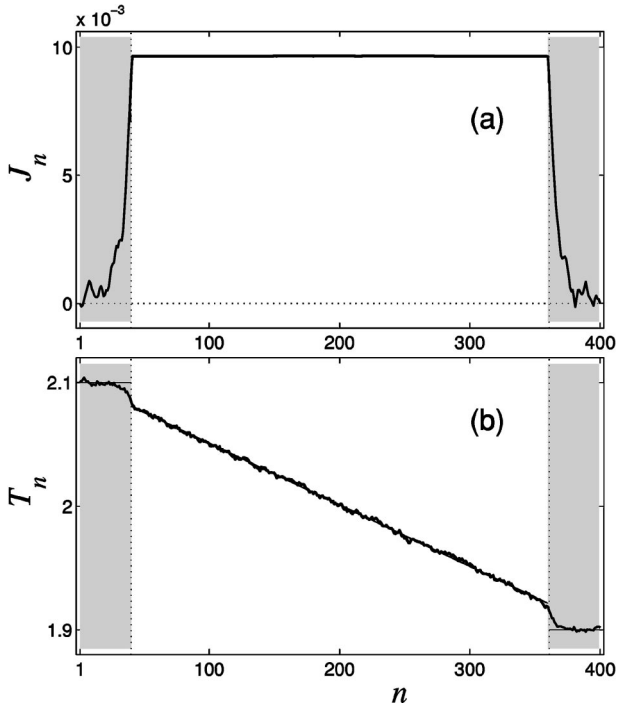

FIG. 2. Distribution of the local heat flux J_n (a) and local temperature T_n (b) in the chain with periodic on-site potential (4), $\epsilon=1$, $N=320$, $N_{\pm}=40$, $T_+=2.1$, $T_-=1.9$. Time of averaging $\tau=10^7$. Fragments of the chain interacting with the thermostats are embedded in gray.

the heat flux is constant ($J_n=J$) and the temperature profile is linear. The coefficient of the heat conductivity can be determined using the information concerning the inner fragment of the chain:

$$\kappa(N)=J(N-1)/(T_{N_++1}-T_{N_++N}), \tag{12}$$

or (with less errors) by fitting a linear function

$$T_n=\frac{\kappa(N)}{J}n+b$$

to the inner fragment of the chain.

The limit value

$$\kappa=\lim_{N\to\infty}\kappa(N) \tag{13}$$

will correspond to the coefficient of the heat conductivity at temperature $T=(T_++T_-)/2$. The question regarding the finiteness of the heat conductivity is reduced to the existence of finite limit (13).

An alternative way to compute the heat conductivity κ is by means of the well known Green-Kubo formula [28]:

$$\kappa=\lim_{\tau\to\infty}\int_0^{\tau}\lim_{N\to\infty}\frac{1}{NT^2}\langle \mathbf{J}(s)\cdot\mathbf{J}(0)\rangle ds, \tag{14}$$

where N is the number of particles in a chain with periodic boundary conditions,

$$\mathbf{J}(\tau)=\sum_{n=1}^{N} j_n(\tau)$$

is the total heat flux, and the averaging $\langle\cdot\rangle$ is performed over all thermalized states of the chain. Consequently, the finiteness of the heat conductivity is related to the convergence of the integral

$$\int_0^\infty C(\tau)d\tau, \tag{15}$$

with

$$C(\tau)=\lim_{N\to\infty}\frac{1}{NT^2}\langle \mathbf{J}(\tau)\cdot\mathbf{J}(0)\rangle.$$

Numerically the above autocorrelation function may be found only for finite chain

$$C_N(\tau)=\frac{1}{NT^2}\langle \mathbf{J}(s)\mathbf{J}(s-\tau)\rangle_s. \tag{16}$$

For large enough values of N the correlation function $C_N(\tau)$ is believed to approximate the function $C(t)$ with acceptable accuracy. In order to get stable results the value $N=4000$ is usually sufficient. More details concerning the computation of the autocorrelation function are presented in section 2 of the Appendix.

The methods for computing the heat conductivity coefficient based on relationships (13) and (14) are complementary and allow mutual verification of the results.

IV. HARMONIC ON-SITE POTENTIAL

The chain with harmonic on-site potential (3) is described by linear equations and therefore is completely integrable. The energy transport is performed by noninteracting phonon modes. The heat flux J does not depend on the chain length N, but only on the temperature difference ΔT. Linear thermal profile is not formed. At the inner part of the chain the temperature is nearly constant $T_n=(T_+ + T_-)/2$ (Fig. 3). Therefore according to Eq. (12), the heat conductivity coefficient diverges. Correspondingly, the average correlation function $C(\tau)$ is constant and integral (15) diverges.

V. PERIODIC ON-SITE POTENTIAL

Characteristic features of dynamics of the chain with periodic on-site potential (4) depend on the values of the temperature. As the temperature is small $T\ll\epsilon$, the on-site potential may be approximated by harmonic single-well potential (3) with $\omega_0=\sqrt{\epsilon}$. The heat transport is governed by weakly interacting phonons. At the temperature $T\sim\epsilon$ the chaotic superlattice of topological solitons is formed and the transport properties change drastically. At very high temperatures $T\gg\epsilon$ the chain is effectively detached from the site and again weakly interacting phonons govern the heat transport. Therefore it is reasonable to investigate the dependence of the heat conductivity on the reduced temperature $\tilde{T}=T/\epsilon$.

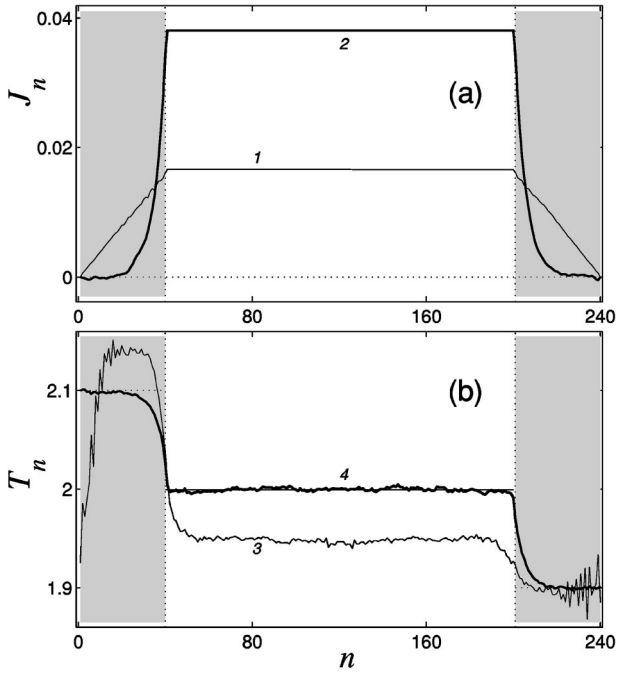

FIG. 3. Distribution of local heat flux J_n (a) and local temperature T_n (b) in the chain with harmonic on-site potential (3), $\omega_0=1$, $N=160$, $N_\pm=40$, $T_+=2.1$, $T_-=1.9$, averaging time $\tau=10^7$. The fragments of the chain interaction with the thermostats are embedded in gray. Thin lines (1,3) are obtained by using the Nosé-Hoover thermostat with $\tau_r=1$, and thick (2,4) by using the Langevin thermostat with $\tau_r=10$.

The behavior of the chain also depends on the cooperativeness parameter $g=1/\epsilon$. The more the cooperativeness, the less is the density of the soliton superlattice and the phonon scattering effects are less significant. The limit $g\to\infty$ $(\epsilon\to 0)$ corresponds to the completely integrable continuum sine-Gordon equation.

Generally, three limits of discrete Frenkel-Kontorova system correspond to the completely integrable systems: at $\tilde{T}\to 0$ the system reduces to the harmonic chain with harmonic on-site potential; at $\tilde{T}\to\infty$ to an isolated harmonic chain; at $g\to\infty$ to the continuous sine-Gordon equation. All these limit systems have diverging heat conductivity. The behavior of the system in the vicinity of these limits is a natural question to be addressed.

Let us start from $g=1$ $(\epsilon=1,\ \tilde{T}=T)$ and investigate the sequence $\kappa(N)$ as N grows ($N=10$, 20, 40, 80, 160, 320, 640) and different values of T. As it is may be suggested from Fig. 4 at small $(T=0.2)$ and large $(T=200)$ temperatures the heat conductivity coefficient $\kappa(N)$ grows as N^α, at $T=20$ as $\ln N$, and at $T=3$ converges to finite value $\kappa=18.5$. Therefore it may be concluded that at $T=3$ the chain has finite heat conductivity. The data related to the other values of the temperature do not allow to draw any conclusions about the behavior of the heat conductivity at larger values of N. Generally speaking, it may happen that for longer chains $\kappa(N)$ will attain certain finite value. Computational tools we use do not allow to investigate higher values

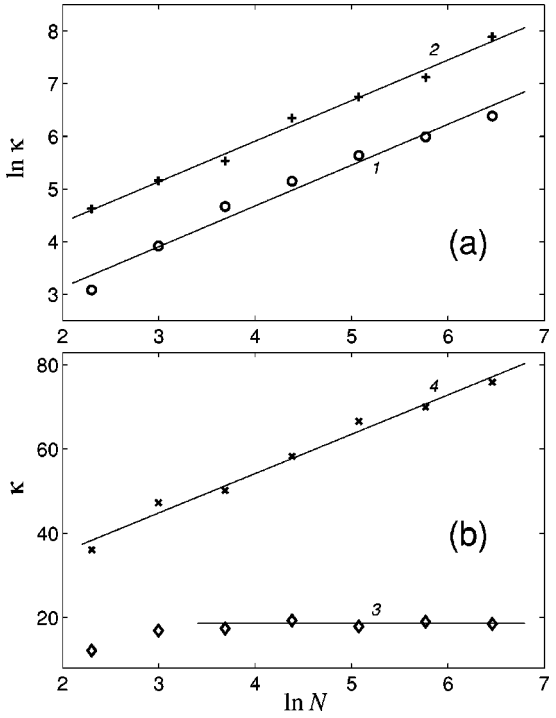

FIG. 4. Dependence of the logarithm of the heat conductivity coefficient $\ln \kappa(N)$ (a) and $\kappa(N)$ (b) on the logarithm of the inner fragment length $\ln N$ ($N_+ = N_- = 40$) for the chain with periodic on-site potential (4), $\epsilon = 1$, $T = 0.2$ (markers 1), $T = 200$ (markers 2), $T = 3$ (markers 3), and $T = 20$ (markers 4). The markers denote the computed values and the lines correspond to the best linear approximations.

of N. Still, it is possible to get additional information from the behavior of the autocorrelation function $C(\tau)$ at $\tau \to \infty$.

Numerical simulation demonstrates that for $T = 3$ the autocorrelation function decreases exponentially (Fig. 5, curve 1). Integral (15) converges and the Green-Kubo formula (14) gives $\kappa = 17.5$, in good correspondence with $\kappa = 18.5$ obtained from direct simulation of the heat flux. At $T = 20$ the autocorrelation function at time scale $0 \leqslant \tau \leqslant 800$ also decreases exponentially (Fig. 5, curve 2). If this trend persists also for $\tau > 800$, the Green-Kubo formula will give κ

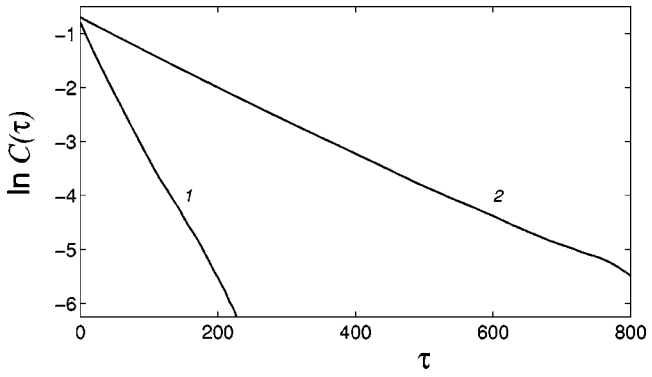

FIG. 5. Exponential decrease of the autocorrelation function $C(\tau)$ in the chain with periodic on-site potential (4), $\epsilon = 1$, $T = 3$ (curve 1) and $T = 20$ (curve 2) (semilogarithmic coordinates).

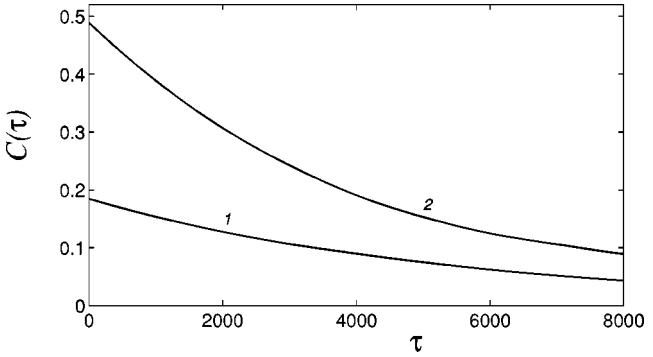

FIG. 6. Autocorrelation functions $C(\tau)$ in the chain with periodic on-site potential (4), $\epsilon = 1$, $T = 0.2$ (curve 1) and $T = 200$ (curve 2).

$= 77.4$. It is reasonable to compare this value with the result for $\kappa(N)$ presented in Fig. 4 (curve 4). Maximum value of $\kappa(640) = 75.9$ and no trend towards any finite limit of $\kappa(N)$ may be detected. Therefore the likely result is divergence. In order to verify this result the simulation for larger values of N (1280, 2560, 5120, 10 240) is required, which is beyond our computational possibilities.

The problem for $T = 0.2$ and $T = 200$ is even more difficult. The autocorrelation function is presented in Fig. 6. The decrease of the function is very slow and no unambiguous conclusion concerning its character may be drawn out. While extrapolating $c(\tau)$ for $\tau > 8000$ by exponent, the Green-Kubo formula yields $\kappa = 1016$ for $T = 0.2$ and $\kappa = 2252$ for $T = 200$. In order to get additional information more detailed simulation is required. Still, from the other side, for $T = 200$ at $N = 640$ the logarithm of the heat conductivity $\ln \kappa(N) = 7.9 > \ln(2252) = 7.7$, and the dependence $\ln \kappa(N)$ (Fig. 4, curve 2) does not demonstrate any trend towards convergence. Therefore the most likely result in this case is also the divergence of the heat conductivity.

Let us consider the sequence $\kappa(N)$ ($N = 10$, 20, 40, 80, 160, 320, 640) at other values of the cooperativeness. The results are summarized in Fig. 7. The space of parameters $(g, \tilde{T})$ is divided in two zones denoted by different colors. In the first (gray) zone the sequence $\kappa(N)$ converges [$\kappa(160) \approx \kappa(320) \approx \kappa(640)$], and in the second (white) zone the sequence grows monotonously. Then, in the first zone Frenkel-Kontorova model has finite heat conductivity, and in the second zone the heat conductivity is either divergent or finite but very high.

The first zone is limited by certain finite value of g: for all g above some $g_0 > 1$ no convergence of $\kappa(N)$ was found. The explanation is that for growing g the behavior of the system should be determined by the continuum limit described by integrable sine-Gordon equation. At any fixed $g < g_0$ for $N \leqslant 640$ the heat conductivity converges only for some finite temperature interval $0 < \tilde{T}_b < \tilde{T} < \tilde{T}_h < \infty$. As the cooperativeness decreases ($g \to 0$), the upper boundary of this interval tends to infinity ($\tilde{T}_h \to \infty$), and the lower boundary tends to zero ($\tilde{T}_b \to 0$) proportionally to g.

The dependence of κ on the reduced temperature $\tilde{T}$ is presented in Fig. 8. Within the interval $[\tilde{T}_b, \tilde{T}_h]$ there exists

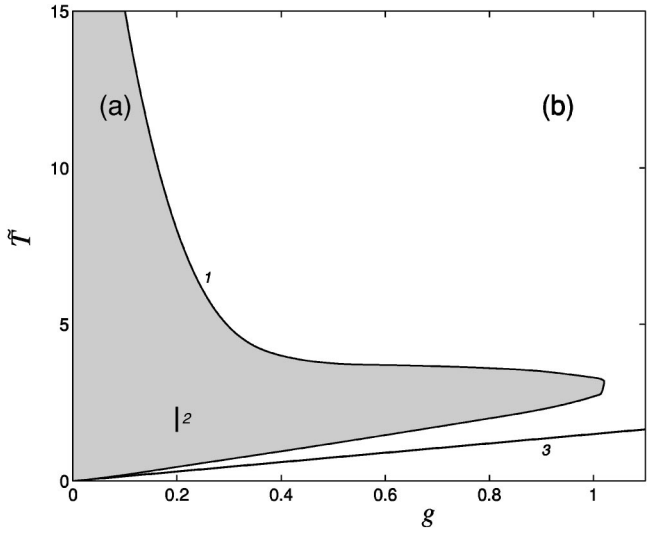

FIG. 7. The zone in the space of parameters $(g,\tilde{T})$, where for finite chains of length $N\leqslant 640$ with on-site potential (4) the heat conductivity converges [(a), gray zone] and diverges [(b), white zone]. Curve 1 divides these two zones. Interval 2 corresponds to the parameters used in Ref. [16]. For finite chains ($N\leqslant 640$) with on-site potential ϕ^4 (5) finite heat conductivity is detected only above line 3.

a critical value $\tilde{T}_m$ corresponding to the minimum of heat conductivity.

In order to reveal the mechanism of the heat conduction it is reasonable to explore the behavior of heat capacity $c=\langle H\rangle/NT$ ($\langle H\rangle$ is the average energy of cyclic N-atomic chain at the temperature T) on the reduced temperature $\tilde{T}$ (Fig. 9). The heat capacity of classic harmonic chain is unity, therefore the deviation of this value from unity characterizes the significance of nonlinear effects. The lattice considered has negative anharmonicity and therefore $c>1$ for all temperatures. The heat capacity tends to unity as $\tilde{T}\to 0$ and $\tilde{T}\to\infty$ and has a single maximum at a certain temperature $\tilde{T}_c$. This value fairly well coincides with the temperature $\tilde{T}_m$, which corresponds to the minimum of the heat conductivity.

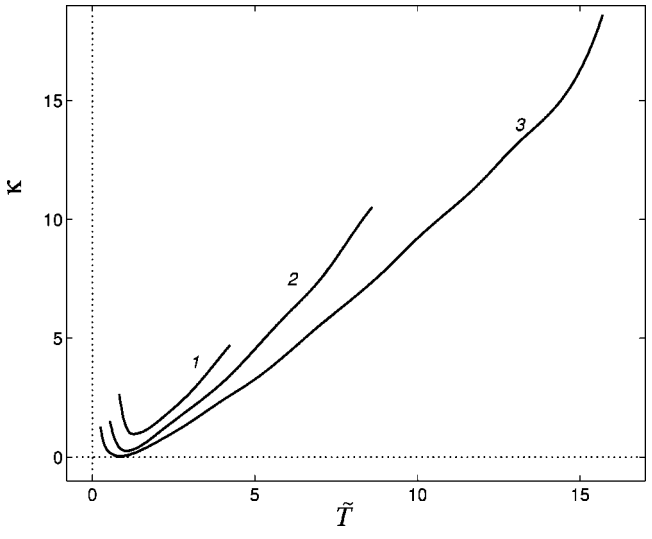

FIG. 8. Dependence of the heat conductivity coefficient κ on the reduced temperature $\tilde{T}=T/\epsilon$ for the chain with periodic on-site potential (4) for $\epsilon=3$ (curve 1), $\epsilon=5$ (curve 2), and $\epsilon=10$ (curve 3).

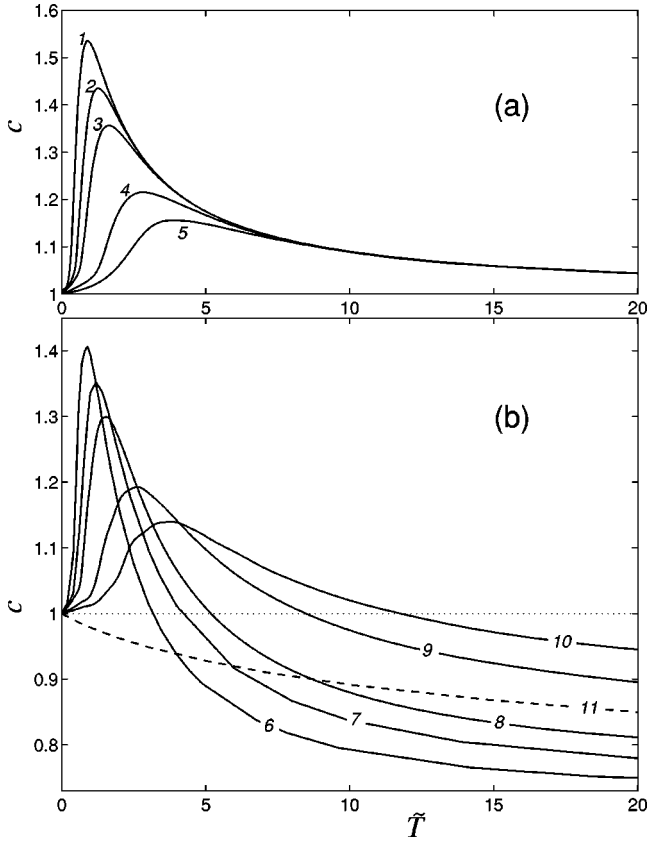

FIG. 9. The dependence of the dimensionless heat capacity c on the reduced temperature $\tilde{T}=T/\epsilon$ (a) for the chain with periodic on-site potential (4) and (b) for the chain with ϕ^4 potential (5) for $\epsilon=10$ (curves 1,6), $\epsilon=5$ (curves 2,7), $\epsilon=3$ (curves 3,8), $\epsilon=1$ (curves 4,9), and $\epsilon=0.5$ (curves 5,10). Dashed curve 11 gives a similar dependence for the chain with on-site sinh-Gordon potential (6), for $\omega_0=1$.

Moreover, the increase and decrease of the heat capacity is clearly correlated with the decrease and increase of the heat conductivity. This fact suggests that the same physical effects are responsible for both processes. For zero temperature the heat capacity is equal to unity. We suppose that the increase of the heat capacity at higher temperatures is related to thermal activation of topological solitonlike excitations (kinks and antikinks) that represent additional degrees of freedom for this system. As a result the dynamical superlattice of solitons appears. The density of this superlattice approaches its maximum at the temperature $\tilde{T}_m$. Further growth of the temperature results in the decrease of the number of degrees of freedom, which is manifested as effective detaching of the chain from the on-site potential. Therefore the heat capacity decreases and tends to unity as the temperature grows.

These correlations between the behavior of the heat capacity and the heat conductivity and especially the fair coincidence of $\tilde{T}_m$ and $\tilde{T}_c$ allow us to suppose that the heat trans-

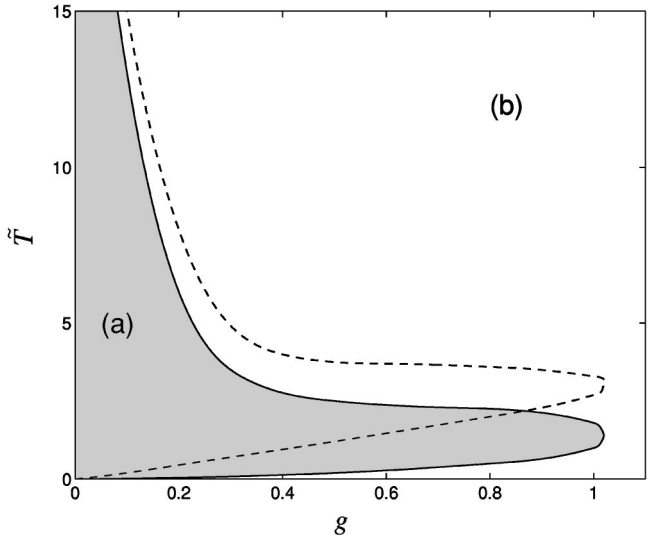

FIG. 10. Zones in the space of parameters $(g,\tilde{T})$, where for the finite chains $N\leqslant 640$ with periodic on-site potential (4) and period $l=2\pi\sqrt{2}$ the heat conductivity is normal [(a), gray] and abnormal [(b), white]. The dashed line denotes the same boundary for the commensurate Frenkel-Kontorova model $(l=2\pi)$.

fer is limited mainly by phonon scattering on the soliton superlattice. The effectiveness of this scattering depends on the density of the superlattice as well as on the ability of single kinks to scatter phonons. In the strongly cooperative regime $g>g_0$ the interaction between kinks and phonons is nearly elastic (close to the case of complete integrability) and therefore the heat conductivity has the trend to grow, probably to infinity. For lower cooperativeness the soliton-phonon interaction is less elastic and the finite range $[\tilde{T}_b,\tilde{T}_h]$ of converging heat conductivity appears. For the cases of $\tilde{T}<\tilde{T}_b$ and $\tilde{T}>\tilde{T}_h$, we could not see convergence of the heat conductivity. The suggested reason for this effect is that the soliton superlattice effectively disappears.

Let us consider now an incommensurate Frenkel-Kontorova chain where the period of the chain is different from the period of the on-site potential. The dimensionless on-site potential is a periodic function (4) with period 2π, and the chain has period $l=2\pi q$. Then function $F(u_n)$ in Eq. (7) will take the form

$$F(u_n)=\frac{d}{du}U(u_n+nl).$$

For the sake of simulation we choose $q=l/2\pi=\sqrt{2}$. It is well known [29] that such a lattice in its ground state already has a soliton superlattice of nonzero density. Therefore the convergence of the heat conductivity is expected to be facilitated as compared to the commensurate case.

Figure 10 demonstrates the zone in the space of parameters $(g,\tilde{T})$ where $\kappa(N)$ seems to converge. For the sake of comparison the boundary for the commensurate case is also presented $(l=2\pi)$. The result is that no qualitative change of the behavior occurs. The only difference is that the zone with normal heat conductivity moves down. This effect is related to the presence of the topological kinks at any temperature. The appearance of normal heat conduction in the current framework occurs at lower temperature since less solitons should be thermally activated in order to achieve convergence. On the other hand, the kink superlattice facilitates effective detachment of the lattice from the on-site potential (the average coupling energy in the ground state is less) and therefore the upper boundary for the normal heat conduction is also achieved at lower temperatures.

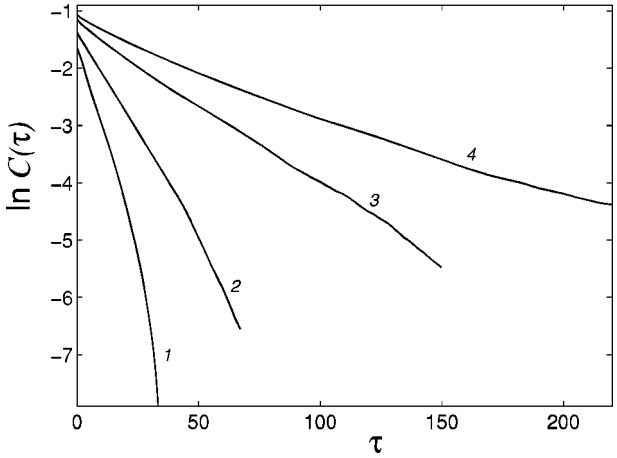

FIG. 11. Exponential decrease of the autocorrelation function $C(\tau)$ in the chain with on-site potential ϕ^4 (5), $\epsilon=1$, $T=20$ (curve 1), $T=10$ (curve 2), $T=5$ (curve 3), and $T=3$ (curve 4). [Semi-logarithmic coordinates $\ln C(\tau)$ versus τ.]

VI. HEAT CONDUCTIVITY OF THE CHAIN WITH DOUBLE-WELL ON-SITE POTENTIAL

Let us consider the heat conductivity of the chain with a ϕ^4 on-site potential (5). For this case $\kappa(N)$ seems to converge when $\tilde{T}>\tilde{T}_0=3g/2$ $(T>1.5)$, see Fig. 7.

In order to investigate the behavior in the temperature range $\tilde{T}<\tilde{T}_0$, let us consider the temperature dependence of

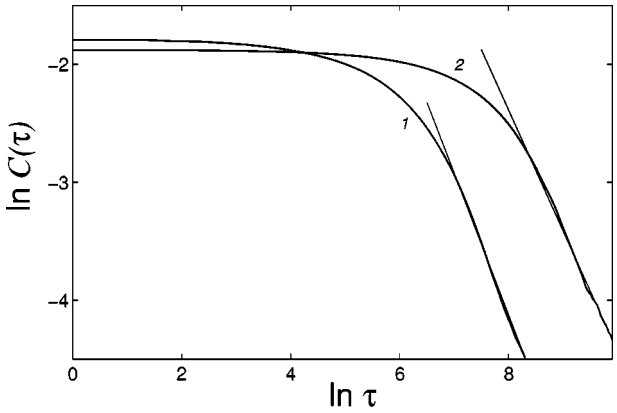

FIG. 12. Power-law decrease of the autocorrelation function $C(\tau)$ in the chain with ϕ^4 on-site potential (5), $\epsilon=1$, $T=1$ (curve 1), and $T=0.5$ (curve 2). [Double logarithmic coordinates $\ln C(\tau)$ versus $\ln\tau$.] The angle coefficient α determines the decrease rate. For $T=1$, $\alpha=1.2$; for $T=0.5$, $\alpha=1.02$.

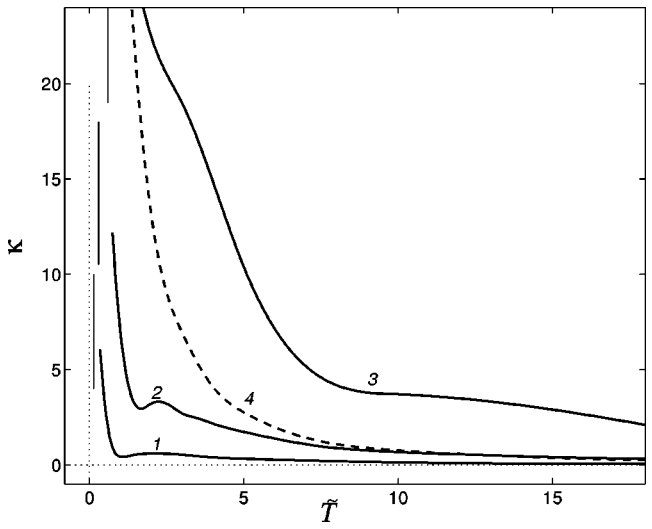

FIG. 13. Heat conductivity κ versus reduced temperature $\tilde{T}=T/\epsilon$ for the chain with double-well on-site potential (5), $\epsilon=4$ (curve 1), $\epsilon=2$ (curve 2), and $\epsilon=1$ (curve 3) and for the chain with sinh-Gordon on-site potential (6), $\omega_0=1$ (dashed curve 4, $\tilde{T}=T$).

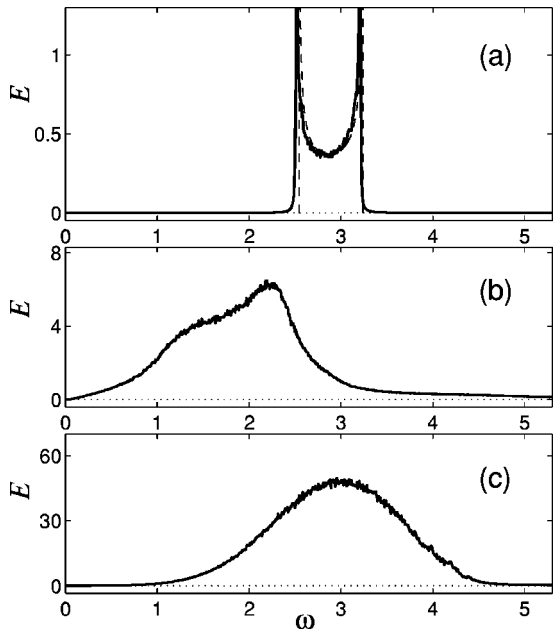

FIG. 14. Frequency spectrum of energy of vibrations in the chain with double-well on-site potential (5) at temperatures $T=0.4$ (a), $T=10$ (b), and $T=100$ (c); $\epsilon=4$. The dashed line denotes the spectrum of harmonic chain (3) with $\omega_0=4/\pi\sqrt{\epsilon}$.

the autocorrelation function $C(\tau)$. For $g=1$ ($\epsilon=1$) this is shown in Fig. 11. As $\tau\to\infty$ the autocorrelation function decreases exponentially. The decrease rate grows as the temperature increases and therefore the conclusion concerning finite heat conductivity at $\tilde{T}>\tilde{T}_0$ is confirmed. At lower temperatures the decrease rate seems to satisfy a power law $\tau^{-\alpha}$—see Fig. 12. The degree α decreases with the decrease of the temperature. At $T=1$, $\alpha=1.2>1$, therefore integral (15) converges and the heat conductivity is finite, at $T=0.5$ we find $\alpha=1.02$. Within the current accuracy this value corresponds to the transition to the abnormal heat conduction. It is extremely difficult to obtain reliable data for lower temperatures in order to substantiate this conclusion because of huge computation time required. The reason is that the system is rather close to the completely integrable case. New numerical methods are needed to investigate this kind of systems.

The dependence of the heat conductivity κ on reduced temperature $\tilde{T}$ is presented in Fig. 13. For low cooperativeness ($g<0.5$) the heat conductivity shows a local minimum and local maximum (at $\tilde{T}=\tilde{T}_1$), before decreasing monotonously to zero as $\tilde{T}\to\infty$. The relative value of the maximum decreases as the cooperativeness grows, and it disappears for a certain critical value of ϵ.

To understand this behavior of the heat conductivity, it is again useful to investigate the behavior of the heat capacity c [Fig. 9(b)]. As $\tilde{T}\to 0$ the heat capacity $c\to 1$. As the temperature grows, the heat capacity grows, achieves its maximum at the temperature $\tilde{T}_c$, and then decreases monotonously to a value less than unity. The value $\tilde{T}_c$ is situated near the maximum point of the heat conductivity $\tilde{T}_1$. Such behavior is related to the peculiarities of ϕ^4 potential. At low temperatures the main effect is due to negative anharmonicity near the ground state (therefore the heat capacity exceeds unity) and for high temperatures ($\tilde{T}\gg 1$) the process is governed by positive anharmonicity, bringing the heat capacity to the value below unity.

Let us now consider the frequency distribution of vibrations of the chain. The spectrum is computed for $\epsilon=4$ ($g=1/4$) and three characteristic temperatures $T=0.4$, 10, 100. The spectrum of the chain with harmonic on-site potential (3) does not depend on the temperature and has the form

$$E(\omega)=2\omega/\pi\sqrt{(\omega^2-\omega_0^2)(\omega_1^2-\omega^2)}, \tag{17}$$

where the maximum frequency is $\omega_1^2=4+\omega_0^2$. For $\epsilon=4$, $\omega_0=4/\pi\sqrt{\epsilon}=2.546$, $\omega_1=3.238$. As it is demonstrated in Fig. 14(a), for temperature $T=0.4$ the spectrum of the chain with on-site ϕ^4 potential nearly coincides with the vibration spectrum of a purely harmonic chain (17). This means that at low temperatures only phonons contribute to the frequency spectrum and other excitations do not play any significant role. For $T=10>\epsilon$ the distribution extends below the lower boundary of the propagation zone ω_0 [Fig. 14(b)]. Such a low-frequency component may be associated with intrinsic vibrations of the solitons superlattice. For even higher temperatures $T=100\gg\epsilon$ the spectrum crosses also the upper boundary of the propagation zone ω_1 [Fig. 14(c)]. Such effect may be attributed only to excitation of high-frequency discrete breathers. Therefore, for low temperatures $\tilde{T}<\tilde{T}_0=0.5g$ the dynamics of the system is close to that of a harmonic chain. The heat transport is governed by weakly interacting phonons and heat conductivity may be divergent. For higher temperatures the heat conductivity converges. In the intermediate range $\tilde{T}_0<\tilde{T}<\tilde{T}_1$ the effective phonon scattering mechanism is due to the superlattice of topological kinks,

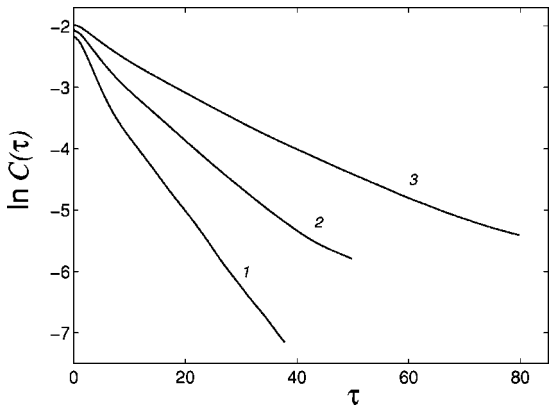

FIG. 15. Exponential decrease of the autocorrelation function $C(\tau)$ in the chain with sinh-Gordon on-site potential (6), $\omega_0=1$, $T=10$ (curve 1), $T=7$ (curve 2), and $T=5$ (curve 3). [Semilogarithmic coordinates $\ln C(\tau)$ versus τ.]

and for high temperatures $\tilde{T}>\tilde{T}_1$ due to high-frequency discrete breathers. Interplay of these two different mechanisms of phonon scattering explains also the dependence of the heat conductivity on the cooperativeness of the system (Fig. 13). The minimum and maximum of the heat conductivity disappear with growth of the cooperativeness since the soliton mechanism of scattering becomes less effective (the soliton-phonon interaction is closer to elastic) and simultaneously the excitation of the discrete breathers becomes easier.

VII. HEAT CONDUCTIVITY OF THE CHAIN WITH sinh-GORDON ON-SITE POTENTIAL

The heat conductivity of this system has been investigated in Ref. [17], and we want to elucidate the detailed physical mechanisms. The on-site potential (6) is a single-well function with positive anharmonicity. The sequence $\kappa(N)$ converges for high temperatures; for low temperatures the accuracy of current experiment is again insufficient. This observation is supported by the fact that the autocorrelation function $C(\tau)$ at high temperatures for $\tau\to\infty$ decreases exponentially (Fig. 15), and for low temperatures by a power law (Fig. 16).

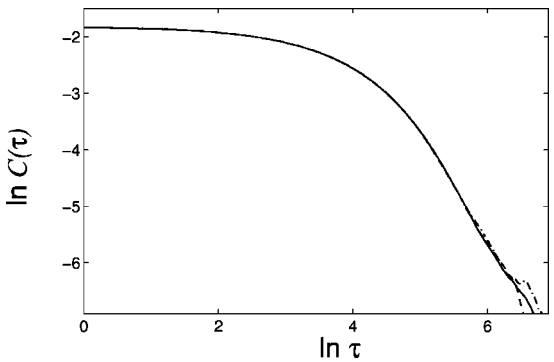

FIG. 16. Power-law decrease of the autocorrelation function $C(\tau)$ in the chain with sinh-Gordon on-site potential (6), $\omega_0=1$, $T=2$. The solid line corresponds to the number of particles $N=500$, dotted line to $N=1000$, and dashed-dotted line to $N=2000$.

The heat conductivity decreases monotonously and for $T\to\infty$ exponentially tends to zero (Fig. 13, curve 4). Positive anharmonism of the potential leads to monotonous decrease of the heat capacity (Fig. 9, curve 11). The frequency spectrum of vibrations moves towards the upper boundary of the propagation zone with growth of the temperature. These facts allow us to conclude that the high-frequency discrete breathers provide effective phonon scattering in this model and facilitate the convergence of the heat conductivity. Growing concentration of these breathers with the growth of the temperature leads to monotonous decrease of the heat conductivity coefficient.

Chain with on-site potential

$$V(u)=\beta u^4/4 \tag{18}$$

(positive ϕ^4 model) also has finite heat conductivity [18,19]. Potential (18), as well as sinh-Gordon on-site potential (6), is a single-well symmetric function with positive anharmonism. Therefore the mechanism of the phonon scattering is also related to the discrete breathers and $\kappa(T)\searrow 0$ for $T\to\infty$. For $\beta=2$ the heat conductivity $\kappa(T)\sim T^{-1.35}$ [19].

VIII. CONCLUSION

The investigation presented above demonstrates that the conductivity of any concrete model of chains with on-site potentials depends on peculiar nonlinear excitations, which determine the process of the heat transfer and phonon scattering. Two typical mechanisms of the phonon scattering were revealed in the paper—thermalized soliton superlattice (discrete sine-Gordon and ϕ^4 models) and discrete high-frequency breathers (ϕ^4 and sinh-Gordon models). Phonon scattering mechanism may switch with the change of the temperature (ϕ^4 model).

For the discrete Frenkel-Kontorova model the zone of the converging heat conductivity for given chain length is limited by low and high temperatures and by high cooperativeness. The numerical possibilities available till date do not allow us to establish unambiguously the character of the heat conductivity outside the zone designated at Fig. 7. Still there is a reason to suggest that an infinite chain has diverging heat conductivity for certain parameters, although the zone corresponding to finite heat conductivity will be larger than computed above. The same is relevant for two other models considered. Still, the transition from an exponential to power-law-like decrease rate of the autocorrelation function is observed in every case. This observation supports the suggestions related to the switches of physical mechanisms responsible for the character of the heat transport.

ACKNOWLEDGMENTS

The authors are grateful to the Russian Foundation of Basic Research (Grant No. 01-03-33122), to the RAS Commission for Support of Young Scientists (6th competition, Grant No. 123), and to the Fund for Support of Young Scientists for financial support. A. V. Savin is grateful to the International Association of Assistance for the promotion of cooperation with scientists from the New Independent States of the

former Soviet Union (project INTAS No. 96-158) for financial support. O.V. Gendelman is grateful to AFOSR (Contract No. 00-AF-B/V-0813) for financial support.

APPENDIX

1. Numerical realization of the Langevin thermostat

System of equations describing the dynamics of the chain attached to thermostats (7) has been integrated numerically by standard fourth-order Runge-Kutta method with constant step of integration $\Delta\tau$. Numerical realization of δ-function is performed as $\delta(\tau)=0$ for $|\tau|>\Delta\tau/2$ and $\delta(\tau)=1/\Delta\tau$ for $|\tau|\leqslant\Delta\tau$, i.e., the step of integration corresponds to the correlation time of the random forces. That is why in order to get correct description of the Langevin thermostat we must guarantee that the relaxation time $\tau_r\gg\Delta\tau$. In order to fulfill this condition the relaxation time was chosen as $\tau_r=10$, and the step of integration for different values of N was chosen as $\Delta=0.05,\ 0.025,\ 0.0125$.

For every step of integration the random forces $\xi_n^{\pm}$ were taken to be constant. They were computed as independent realizations of the random value ξ, normally distributed with zero average $\langle\xi\rangle=0$ and dispersion $\langle\xi^2\rangle=2T_{\pm}/\tau_r\Delta\tau$. For generating the random value ξ, program package ZUFALL [30] was used.

The initial state for the integration of Eqs. (7) was chosen to be equal to ground state of the chain:

$$u_n=u_0,\quad u_n'=0,\quad n=1,2,\ldots,N_++N+N_-, \tag{A1}$$

where $u_0=0$ for on-site potentials (3) and (6) and $u_0=\pi$ for potentials (4) and (5). It is convenient to control the accuracy of the simulation through the behavior of a sequence of average local heat fluxes $\{J_n\}_{n=N_++1}^{N_++N}$. If the choice of the integration step $\Delta\tau$ is correct then this sequence should be constant. If the local average heat flux changes from particle to particle then the integration step should be reduced. For growing chain length N the step of integration should be also reduced in order to provide sufficient accuracy; the averaging time also grows (see Ref. [31]) and therefore the time of simulation necessary for obtaining reliable results for large N turns out to be extremely large.

2. Computation of the correlation function

In order to compute the autocorrelation function of the heat flux $C_N(\tau)$ the dynamics of cyclic N-particle chain was simulated. The thermalized chain with temperature T was obtained by integrating Langevin system of equations,

$$u_n''=u_{n+1}-2u_n+u_{n-1}-F(u_n)-\gamma u_n'+\xi_n,$$

$$n=1,2,\ldots,N, \tag{A2}$$

where $n+1=1$ for $n=N$ and $n-1=N$ for $n=1$, $\gamma=0.1$ (relaxation time $\tau_r=10$), ξ_n represents white Gaussian noise normalized as

$$\langle\xi_n(\tau)\rangle=0,\quad \langle\xi_n(\tau_1)\xi_k(\tau_2)\rangle=2\gamma T\delta_{nk}\delta(\tau_2-\tau_1).$$

System (A2) has been integrated numerically with initial conditions corresponding to the ground state of the chain. After time $\tau=10\tau_r$ the chain approached equilibrium with the thermostat and the coordinates

$$\{u_n(\tau),u_n'(\tau)\}_{n=1}^{N} \tag{A3}$$

corresponding to the thermalized state at temperature T.

Afterwards, the dynamics of isolated thermalized chain was simulated. For this purpose system (A2) was integrated with zero damping $\gamma=0$ and zero external force $\xi_n\equiv0$). Thermalized state (A3) was used as initial condition. The result was the dependence of the general heat flux **J** on time τ. Afterwards with the help of Eq. (16) the autocorrelation function $C_N(\tau)$ was computed for given thermalized state of the chain. The autocorrelation function depends significantly on concrete realization of the thermalized chain. That is why in order to improve the accuracy this procedure was performed 10^3–10^4 times with independent initial realizations of the thermalized state. Finally, the shape of the correlation function was computed as average over all these realizations. It is worth mentioning that the alternative way of computation (performing of one very large simulation) would not bring about any sufficient gain in the accuracy because of growing integration errors.

In order to verify the independence of the correlation function on the chain length the appropriate calculations were performed for different values of N. Figure 16 demonstrates the function $C_N(\tau)$ for the chain with sinh-Gordon on-site potential for $\omega_0=1$, $T=2$, and $N=500$, 1000, 2000. It is clear that the autocorrelation function is nearly independent of N (the differences are noticeable only for large times and are reduced as the number of realizations used for averaging grows). For the given set of parameters $N=1000$ provides sufficient accuracy.

3. Comparison of Langevin and Nosé-Hoover thermostats

Unlike the Langevin thermostat, the Nosé-Hoover thermostat (NHT) [25] is not stochastic. Its dynamics is completely determined by the initial conditions. It turned out to be good choice for simulations of FPU system [2,3] but its deterministic nature can bring about artifacts in the behavior of the system. We compare this thermostat with the Langevin thermostat (LT) we use for the case of Frenkel-Kontorova model.

Let us consider the chain with fixed ends ($1<n<N+N_++N_-$) with $N_\pm$ particles attached to NHT having the temperature $T_\pm$. The dynamics of the system is described by

$$u_n''=u_{n+1}-2u_n+u_{n-1}-F(u_n)-\eta_+u_n',$$

$$n=2,\ldots,N_+,$$

$$\eta_+'=\frac{1}{\tau_r^2}\left(\frac{1}{(N_+-1)T_+}\sum_{n=2}^{N_+}u_n'^2-1\right)$$

$$u_n''=u_{n+1}-2u_n+u_{n-1}-F(u_n), \tag{A4}$$

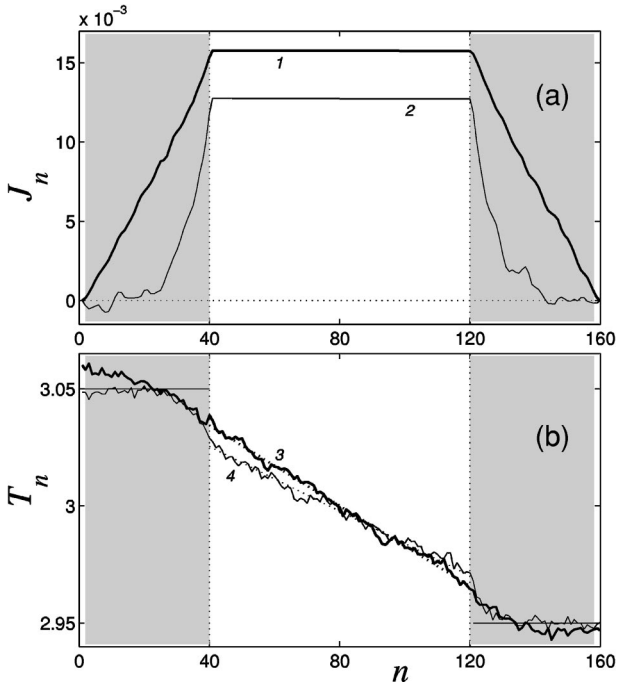

FIG. 17. Distribution of local heat flux J_n (a) and and local temperature T_n (b) in the chain with periodic on-site potential (4), $\epsilon=1$, $N=160$, $N_{\pm}=40$, $T_+=3.05$, $T_-=2.95$, averaging time $\tau=10^7$. Gray zones denote the chain fragments embedded in the thermostats. Thick lines (1, 3) correspond to NHT ($\tau_r=1$), and thin lines (2, 4) to LT ($\tau_r=10$).

$$n=N_+ +1,\ldots,N_+ +N,$$

$$u_n''=u_{n+1}-2u_n+u_{n-1}-F(u_n)-\eta_- u_n',$$

$$n=N_+ +N+1,\ldots,N_+ +N+N_- -1,$$

$$\eta_-'=\frac{1}{\tau_r^2}\left(\frac{1}{(N_--1)T_-}\sum_{n=N_++N+1}^{N_++N+N_-}u_n'^2-1\right),$$

where $F(u)=dU(u)/du$, and τ_r is the relaxation time of the thermostat.

Usually the simulations of the heat conductivity [2,3,16,18] take $\tau_r=1$, and $N_+=N_-=2$ (only end particles are attached to the thermostat $n=2$ and $n=N_++N+N_--1$). But, as stated in Ref. [26], such thermostats are not enough random–they cover only a part of the phase space and correspond to strange attractors. In order to reduce this effect we attach to the thermostat $N_+=N_-=40$ particles from every side of the chain.

The dynamics of system (A4) is also completely deterministic. It should be mentioned that it is impossible to use the initial condition (A1) corresponding to ground state of the system [it is stationary point of system (A4)]. We take the initial condition

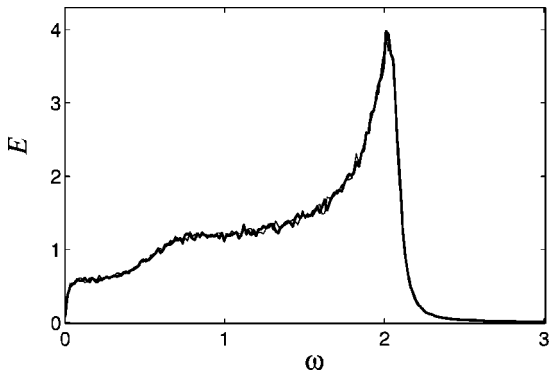

FIG. 18. Frequency distribution of the energy of particle having number $N/2$ in the chain with periodic on-site potential (4), $\epsilon=1$, $N=160$, $N_{\pm}=40$, $T_+=3.05$, $T_-=2.95$. The thick line corresponds to use of NHT ($\tau_r=1$), and thin line to use of LT ($\tau_r=10$).

$$u_n=u_0,\quad u_n'(0)=4\left(\xi_n-\frac{1}{2}\right)\sqrt{(T_++T_-)/2},\quad \text{(A5)}$$

where ξ_n represents independent realizations of the random variable over the interval [0,1].

We choose $\epsilon=1$ ($g=1$), $T_+=3.05$, $T_-=2.95$, $N=80$ and integrate system (A4) numerically with initial condition (A5). The distribution of heat fluxes J_n and local temperatures T_n is presented in Fig. 17 (for the sake of comparison we present also the results obtained by using LT, thin lines). Within the left thermostat the heat flux grows linearly and within the other thermostat it decreases linearly with n. At central part of the chain the value of the heat flux does not depend on n. Linear temperature profile is formed and the heat conductivity coefficient may be computed according to Eq. (12)—$\kappa(N)=18.4$. Use of LT gives $\kappa(N)=18.5$ (see above), i.e., the value of κ does not depend on the type of the thermostat.

In addition, it is possible to conclude from Fig. 18 that the frequency distribution of the energy of vibrations also does not depend on the type of thermostat used. It means that for the case of the temperatures close to the value of the potential barrier the choices of NHT or LT bring about equivalent results

The situation is strikingly different if the temperature is lower and the chain is closer to the linear case. The Nose-Hoover thermostat is not effective in this case. In order to illustrate this fact we use the model of harmonic chain. As it is clear from Fig. 3, NHT gives values of the heat flow substantially different from the correct values; at the same time the use of LT secures much better results. That is why in the present paper we used more complicated and consuming LT.

It should be mentioned that sometimes due to its simplicity NHT is used in combination with LT [32] (LT is used for the parameters of the model where NHT is not acceptable).

[1] E. Fermi, J. Pasta, and S. Ulam, Los Alamos Report No. LA-1940, 1955 (unpublished).
[2] S. Lepri, R. Livi, and A. Politi, Phys. Rev. Lett. **78**, 1896 (1997).
[3] S. Lepri, R. Livi, and A. Politi, Physica D **119**, 140 (1998).
[4] S. Lepri, R. Livi, and A. Politi, Europhys. Lett. **43**, 271 (1998).
[5] R. Rubin and W. Greer, J. Math. Phys. **12**, 1686 (1971).
[6] A. Casher and J.L. Lebowitz, J. Math. Phys. **12**, 1701 (1971).
[7] A. Dhar, Phys. Rev. Lett. **86**, 5882 (2001).
[8] A. Dhar, Phys. Rev. Lett. **86**, 3554 (2001).
[9] A.V. Savin, G.P. Tsironis, and A.V. Zolotaryuk, Phys. Rev. Lett. **88**, 154301 (2002).
[10] P. Grassberger, W. Nadler, and L. Yang, Phys. Rev. Lett. **89**, 180601 (2002).
[11] G. Casati and T. Prosen, e-print cond-mat/0203331.
[12] T. Hatano, Phys. Rev. E **59**, R1 (1999).
[13] G. Casati, J. Ford, F. Vivaldi, and V.M. Visscher, Phys. Rev. Lett. **52**, 1861 (1984).
[14] T. Prosen and M. Robnik, J. Phys. A **25**, 3449 (1992).
[15] M.J. Gillan and R.W. Holloway, J. Phys. C **18**, 5705 (1985).
[16] B. Hu, B. Li, and H. Zhao, Phys. Rev. E **57**, 2992 (1998).
[17] G.P. Tsironis, A.R. Bishop, A.V. Savin, and A.V. Zolotaryuk, Phys. Rev. E **60**, 6610 (1999).
[18] B. Hu, B. Li, and H. Zhao, Phys. Rev. E **61**, 3828 (2000).
[19] K. Aoki and D. Kuznezov, Phys. Lett. A **265**, 250 (2000).
[20] F. Bonetto, J.L. Lebowitz, and L. Ray-Bellet, in *Mathematical Physics 2000*, edited by A. Fokas, A. Grigoryan, T. Kibble, and B. Zegarlins (Imperial College, London, 2000), p. 128.
[21] S. Lepri, R. Livi, and A. Politi, cond-mat/0112193.
[22] C. Giardina, R. Livi, A. Politi, and M. Vassalli, Phys. Rev. Lett. **84**, 2144 (2000).
[23] O.V. Gendelman and A.V. Savin, Phys. Rev. Lett. **84**, 2381 (2000).
[24] A.V. Savin and O.V. Gendelman, Fiz. Tverd. Tela (St. Petersburg) **43**, 341 (2001) [Phys. Solid State **43**, 355 (2001)].
[25] S. Nosé, J. Chem. Phys. **81**, 511 (1984); W.G. Hoover, Phys. Rev. A **31**, 1695 (1985).
[26] A. Fillipov, B. Hu, B. Li, and A. Zeltser, J. Phys. A **31**, 7719 (1998).
[27] K. Aoki and D. Kusnezov, Phys. Rev. Lett. **86**, 4029 (2001).
[28] R. Kubo, M. Toda, and N. Hashitsume, Springer Ser. Solid-State Sci. **31**, 185 (1991).
[29] V.L. Pokrovsky and A.L. Talapov, Zh. Eksp. Teor. Fiz. **75**, 1151 (1978) [Sov. Phys. JETP **75**, 1151 (1978)].
[30] W.P. Petersen, Int. J. High Speed Comput. **6**(3), 387 (1994), ftp://ftp.netlib.org/random/zufall.f
[31] A. Dhar, Phys. Rev. Lett. **87**, 069401 (2001).
[32] M. Terraneo, M. Peyrard, and G. Casati, Phys. Rev. Lett. **88**, 094302 (2002).